AIAA JOURNAL
Vol. 39, No. 2, February 2001

Hole/Crack Identification by Static Strains from Multiple Loading Modes

Chyanbin Hwu* and Y. C. Liang†
National Cheng-Kung University, Tainan 70101, Taiwan, Republic of China

A method using static strains measured from multiple loading modes for the identification of holes and cracks in linear anisotropic elastic materials is introduced. Because of the localized effects of holes/cracks, their existence may not be clearly reflected by a single set of remotely measured boundary strains. By the combining of the concept of multiple loading modes with the technique of nonlinear optimization, several examples of hole/crack identification have been done. During the iteration procedure, the values of the static strains corresponding to the assumed hole/crack geometry and location are obtained by using a recently developed boundary element, which is for linear anisotropic elastic materials and has also been extended to piezoelectric materials. The identified results show that our method for hole/crack identification is stable and accurate for the model problem considered and shows that the method has promise for more complex problems. In addition, the generality of hole profile, the tolerance of measurement error, the spacing and arrangement of sensors, and the flexibility of multiple loading modes are all discussed in detail.

I. Introduction

NO matter how carefully the load-carrying structural system (such as aircraft structures, turbines and rotors, etc.) is designed, there are instances of cracks or structural damage occurring during service. Because cracks may grow under fatigue loading and catastrophic damage may occur after a critical crack length, periodical inspection during systems operating life becomes necessary. To avoid further destruction, one may wish to know in a nondestructive manner the location and the size of the crack. Such information about the crack geometry is indispensable for estimating the safety of the structure. In engineering practice, one usually carries out measurements, using techniques such as ultrasonics, magnetic flux leakage, x rays, penetrant, eddy current, etc.,[1] on the exterior boundary of the body to locate the crack. In the literature, dynamic response is often used to make measured modes and serves as the standard of identification.[2–8] However, the characteristics of vibration modes and frequencies are not always reliable.[7–9]

Current development in smart materials has improved conventional composite materials to self-monitor during service. The massless sensor of a microelectromechanical system makes it possible to embed the sensor successfully into the composite material without changing the original system. For an ideal online identification, the measured values of sensors are obtained during service and not from the laboratory. For this reason, using the boundary data from static deformation as the identification input has gradually become an area of interest for research.[10–15] However, the localized characteristics of the hole/crack effects diminish the progress of identification, especially when the structures are composed of composite materials. In 1993, Kubo et al. identified a crack in a plate through the multiple current method.[16] Bryan and Vogelius[17] measured the boundary voltages induced by certain specified two-electrode current fluxes to reconstruct the locations of a collection of linear cracks. Their research hints that the parameter sensitivities of holes or cracks differ under different loading modes. Therefore, the concept of multiple loading modes is introduced in this paper, identifying not only size but also location and orientation of holes or cracks in composite structures.

Received 2 March 1999; revision received 9 May 2000; accepted for publication 27 June 2000.

*Professor, Institute of Aeronautics and Astronautics; chwu@mail.ncku.edu.tw.

†Ph.D. Student, Institute of Aeronautics and Astronautics; currently Assistant Professor, P.O. Box 90277-4, Department of Aeronautics and Astronautics, China Air-Force Academy, GangShan, Kaohsiung 820, Taiwan, Republic of China.

The determination of the unknown internal hole/crack in a structure for which the boundary values are prescribed (measured experimentally) belongs to the category of inverse problems in mechanics. Because the measured data are usually provided on the exterior boundary, the boundary integral technique[18] for the analysis of the forward mechanics problems has become a promising computational tool, for example, see Refs. 19 and 20. In this paper, a special boundary element developed by Hwu and Yen[21] is employed for the forward analysis. For the inverse problems, nonlinear optimization[22] is an attractive technique that provides a rational and ordered approach to cope with extreme value problems. Examples of the application of this technique to damage detection may be found in Refs. 10, 11, 14, 15, and 17. In this paper, the nonlinear optimization technique is combined with the concept of the multiple loading modes to improve the convergence of the identification.

II. Selection of Sensitive Parameters

The purpose of this paper is to explore the feasibility of identifying a hole/crack by using only the data from static deformation. From the study of Liang and Hwu[23] of piezoelectric materials, we see that stress intensity factors are very insensitive to the crack location especially when the crack size is under a certain value. Similar results may occur for conventional fiber-reinforced composite materials. To be successful in identification, we should be very careful about the choice of parameters that need to be sensitive to the hole/crack size, location, and orientation. Proper selection of the sensitive parameters may speed the search of the extreme value in the inverse problem. Besides the sensitivity, the convenience for practical implementation will also be considered. The basic measured data for the static deformed bodies are the strains and displacements. From these data one may evaluate the stresses, the stress intensity factors (SIF) for cracks, or the stress concentration factors (SCF) for holes. From the viewpoint of convenience, we study the possibility of selecting sensitive parameters that are functions of the basic measured data such as strains, or other well-known parameters such as SIF, SCF, etc.

To determine the variation of strain, SIF, and SCF with respect to hole/crack size, location, and orientation, we first select a suitable computational tool for the mechanical analysis of hole/crack problems. Among several finite element and boundary element methods, we choose the special boundary element method developed by Hwu and Yen.[21] This method deals with two-dimensional anisotropic elastic plates containing a traction-free elliptical hole or crack subjected to in-plane and/or antiplane loadings. This method is more efficient and accurate than the conventional boundary element because its embedded fundamental solution has satisfied the traction-free boundary conditions around the hole/crack surface and because no meshes are needed for the hole/crack boundary. Because of its

performance, it has been extended to several interesting cases such as multiple holes/cracks/inclusions;[24] piezoelectric materials,[25] nonelliptical holes,[26–28] traction-prescribed holes,[29] etc. The success of this method is mostly due to the finding of special fundamental solutions for specific problems, which were derived by using Stroh's complex variable formulation[30] (also see Ref. 31) for anisotropic elasticity. When these fundamental solutions are embedded in the usual boundary integral equation,[18] that is,

$$c_i(\boldsymbol{x}^*)u_j(\boldsymbol{x}^*) + \int_{B+L} p^*_{ij}(\boldsymbol{x}^*, \boldsymbol{x})u_j(\boldsymbol{x})\, \mathrm{d}\Gamma(\boldsymbol{x}) = \int_{B+L} u^*_{ij}(\boldsymbol{x}^*, \boldsymbol{x})\, p_j(\boldsymbol{x})\, \mathrm{d}\Gamma(\boldsymbol{x}) \tag{1}$$

a series of boundary elements were developed. Detailed derivation may be found in the Refs. 21, 24–29, and 32. In Eq. (1), u_j and p_j are the displacements and tractions. Here, $u^*_{ij}(\boldsymbol{x}^*, \boldsymbol{x})$ and $p^*_{ij}(\boldsymbol{x}^*, \boldsymbol{x})$ are the displacements and tractions in the j direction, respectively, at point $\boldsymbol{x}$ corresponding to a unit point force acting in the i direction applied at point $\boldsymbol{x}^*$ and are the fundamental solutions. B and L are the contours of the outer boundary and hole/crack boundary. For a smooth boundary, $c_{ij} = \delta_{ij}/2$, where δ_{ij} is the Kronecker delta. For practical application, however, c_{ij} together with the corresponding principal value can be indirectly computed by letting $u_j = 1$ (and, hence, $p_j = 0$) in Eq. (1).

Having a proper computational tool, we now define our problems as shown in Fig. 1 in which eight sensors are embedded around a rectangular plate and the hole/crack size, location, and orientation are represented by (a, b, x, y, θ). Three different loading modes (see Fig. 2) are considered. One is the tensile loading mode (mode I), and the other two are shearing mode (mode II) and tearing mode (mode III). From a series of convergence studies, only 20 nodes and 16 elements are needed in each example, and its corresponding CPU time for Pentium-166 is about 4 s.

In the following examples, the material properties are selected to be orthotropic and are $E_1 = 114.8$ and $E_2 = 11.72$ GPa, $G_{12} = 9.65$ GPa, and $\nu_{12} = 0.21$. For the isotropic materials, the material properties are $E = 68$ GPa, $G = 25.758$, and $\nu = 0.32$. For the anisotropic materials, the properties are $E_1 = 145$, $E_2 = 20$, and $E_3 = 10.7$ GPa; $G_{23} = 3.6$, $G_{12} = 4.5$, and $G_{13} = 4.5$ GPa; $\nu_{12} = 0.31$, $\nu_{13} = 0.31$ and $\nu_{23} = 0.23$. For piezoelectric material (PZT4), they are $S_{11} = 10.9$, $S_{12} = -5.42$, $S_{13} = -2.10$, $S_{33} = 7.90$, $S_{44} = 19.3$, and $S_{66} = 32.64\ 10^{-12}$ m^2/N; $g_{13} = -11.1$, $g_{33} = 26.1$, and $g_{15} = 39.4 \times 10^{-3}$ Vm/N; and $\varepsilon_{11} = 8.69$ and $\varepsilon_{33} = 7.66 \times 10^7$ V^2/N. The uniform loading applied on the upper edge of the plate is 1 Pa for each loading mode if not specifically mentioned. The lower edge of the plate is fixed, while the other two side edges are free. With the usual definition, the stress intensity factors K_{I}, K_{II}, and K_{III} for cracks and the stress concentration factor SCF for holes may be expressed as[33,34]

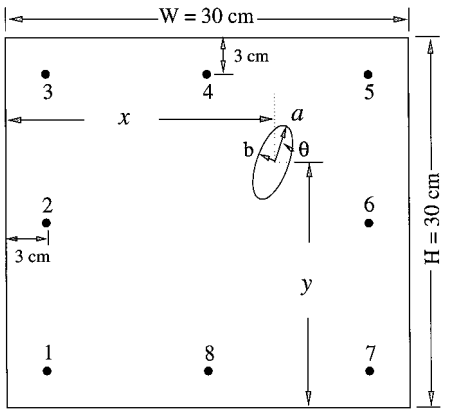

Fig. 1 Definition of hole size, location and orientation, plate size, and sensor position.

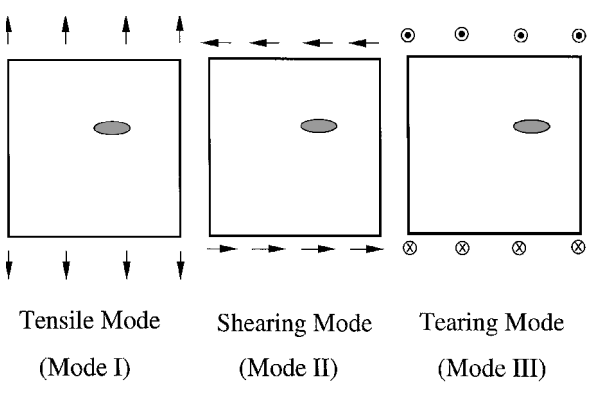

Fig. 2 Three different loading modes.

$$\boldsymbol{K} = \begin{Bmatrix} K_{\mathrm{II}} \\ K_{\mathrm{I}} \\ K_{\mathrm{III}} \end{Bmatrix} = \lim_{r \to 0} \sqrt{2\pi r} \begin{Bmatrix} \sigma_{21} \\ \sigma_{22} \\ \sigma_{23} \end{Bmatrix} \tag{2}$$

$$\mathrm{SCF} = (\sigma_{nn})_{\max}/\sigma_0 \tag{3a}$$

in which r is the distance ahead of the crack tip, σ_{nn} is the hoop stress along the hole boundary, and σ_0 is the uniform load applied at remote boundary. Note that in the following examples, we did not calculate the maximum value of σ_{nn} because it is time consuming. Instead, we calculate σ_{nn} for a specific point. Thus, we use SCF_A to denote the stress concentration factor at point A, that is,

$$\mathrm{SCF}_A = (\sigma_{nn})_A/\sigma_0 \tag{3b}$$

By the preceding definition, the calculation of K_{I}, K_{II}, K_{III}, and SCF depends on the stresses near the crack tip and hole boundary. However, the abrupt change of stresses near holes, especially near the crack tip, may lead to an unavoidable error. To overcome this difficulty, very fine meshes near the hole boundary and crack tips are usually needed when using the conventional finite element or boundary element method. This is not only time consuming but also inaccurate. Recently, through the use of a special boundary element, a closed-form solution for $\boldsymbol{K}$ and σ_{nn}, expressed in terms of remote boundary displacements $\boldsymbol{u}_n$ and tractions $\boldsymbol{t}_n$, has been derived.[28] The solutions are

$$\boldsymbol{K} = \sum_{n=1}^{N} \left\{ \left[\boldsymbol{R}^T \boldsymbol{G}^*_{n1} + \boldsymbol{T}\boldsymbol{G}^*_{n2} \right] \boldsymbol{t}_n - \left[\boldsymbol{R}^T \boldsymbol{Y}^*_{n1} + \boldsymbol{T}\boldsymbol{Y}^*_{n2} \right] u_n \right\} \tag{4}$$

$$\sigma_{nn} = \sum_{n=1}^{N} \{ [\Omega_1 \boldsymbol{G}_{n,1} + \Omega_2 \boldsymbol{G}_{n,2}] \boldsymbol{t}_n - [\Omega_1 \hat{\boldsymbol{Y}}_{n,1} + \Omega_2 \hat{\boldsymbol{Y}}_{n,2}] \boldsymbol{u}_n \}$$

$$\Omega_1 = \boldsymbol{n}^T (\cos\theta \boldsymbol{Q} + \sin\theta \boldsymbol{R}^T), \qquad \Omega_2 = \boldsymbol{n}^T (\cos\theta \boldsymbol{R} + \sin\theta \boldsymbol{T}) \tag{5}$$

in which $\boldsymbol{G}$ and $\boldsymbol{Y}$ are the matrices of influence coefficients and $\boldsymbol{Q}$, $\boldsymbol{R}$, and $\boldsymbol{T}$ are the matrices related to the elasticity constants C_{ijkl}. In the preceding equation $\boldsymbol{n}$ is the unit vector tangent to the hole boundary. Detailed definition and derivation may be found in Ref. 28.

To consider the variation of strains, we define strain functions S_{I}, S_{II}, and S_{III} for each loading mode as

$$S_{\mathrm{I}} = \sum_{l=1}^{8} \left(\frac{\varepsilon_{11}}{\varepsilon^0_{11}} - 1 \right)^2_l, \qquad S_{\mathrm{II}} = \sum_{l=1}^{8} \left(\frac{\varepsilon_{12}}{\varepsilon^0_{12}} - 1 \right)^2_l$$

$$S_{\mathrm{III}} = \sum_{l=1}^{8} \left(\frac{\varepsilon_{13}}{\varepsilon^0_{13}} - 1 \right)^2_l \tag{6}$$

in which ε^0_{ij}, $ij = 11, 12, 13$, are the strain values of the reference problem. To avoid any numerical ill conditioning, the value of $\varepsilon_{ij}/\varepsilon^0_{ij}$ should be normalized to be on the order of unity. To achieve this, we choose the reference problem to have the same geometry and loading conditions as the considered problems except that the hole/crack size and location are different and can be selected arbitrarily because the exact size and location are unknown before the hole/crack detection. In the following examples, the crack/hole size of the reference problem is selected to be $a = 0.5$ cm for cracks or $a = b = 0.5$ cm for holes, and they are located at the center of the plate. The subscript l

($l = 1$–8) of Eq. (6) denotes the sensor location, which is shown in Fig. 1.

Variation with Respect to Hole/Crack Size and Location

Figure 3 shows the variation of the right tip stress intensity factor K_i with respect to the crack size a and location $(x/W, y/W)$ under three different loading modes. The crack orientation for all cases is fixed at the horizontal direction. From Fig. 3, we see that the larger the crack length the higher the stress intensity factors. The variation of the crack location also influences the stress intensity factors. However, the variance under loading modes I and III are not big enough, especially when the crack size is under a certain value such as $a = 2.0$ cm in Fig. 3. Similar phenomena occur for SCF_A in hole problems, which is shown in Fig. 4. As to the variation of strain function S_i with respect to the crack/hole size a and location $(x/W, y/W)$, the results are presented in Figs. 5 and 6. They show distinct variance for mode I loading, but are not sensitive enough for modes II and III. This phenomenon is similar to that shown in Figs. 3 and 4, but the sensitive loading mode is changed from mode II to mode I. Therefore, under the consideration of location and size sensitivity, SCF_A/K_i ties with S_i to be a candidate for hole/crack identification. However, S_i can be applied to both crack and hole problems and can be obtained directly from measurement. It seems that S_i is more appropriate than K_i and SCF_A.

Note that the figures shown here are presented by three different loading conditions. To put all of the data from different loading modes into one figure, the uniform loading σ_0 has been changed to

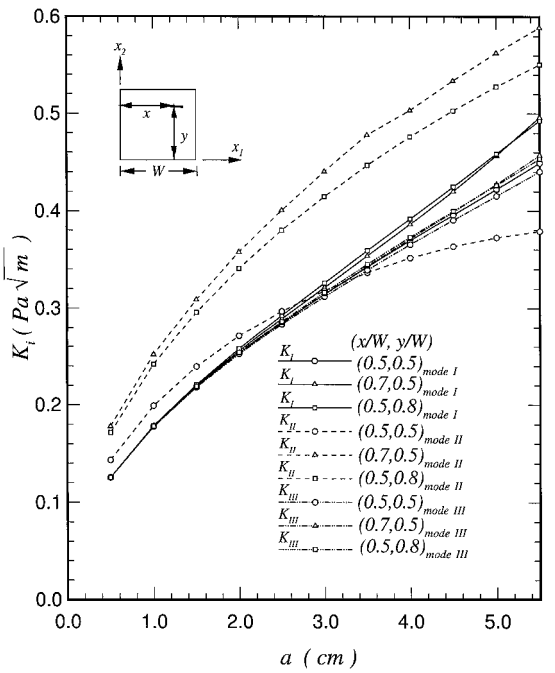

Fig. 3 Variation of the right tip stress intensity factor K_i with respect to the crack size a and location $(x/W, y/W)$, where $\theta = 0$.

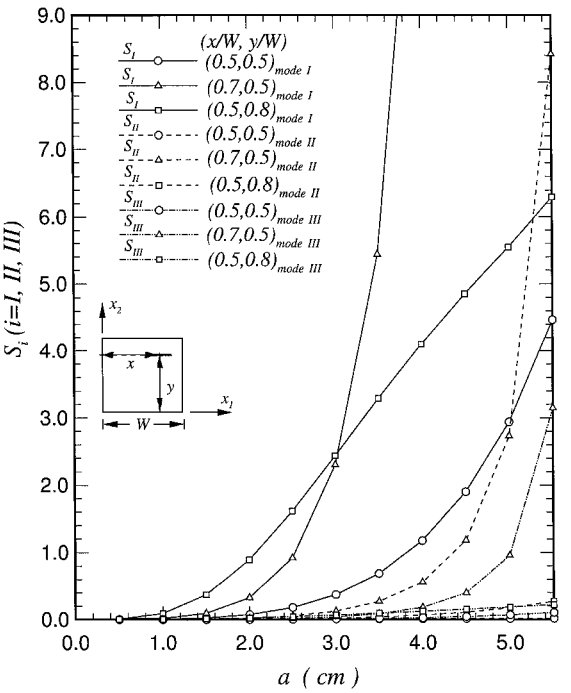

Fig. 5 Variation of the strain functions S_i (i = I, II, III) with respect to the crack size a and location $(x/W, y/W)$, where θ = 0.

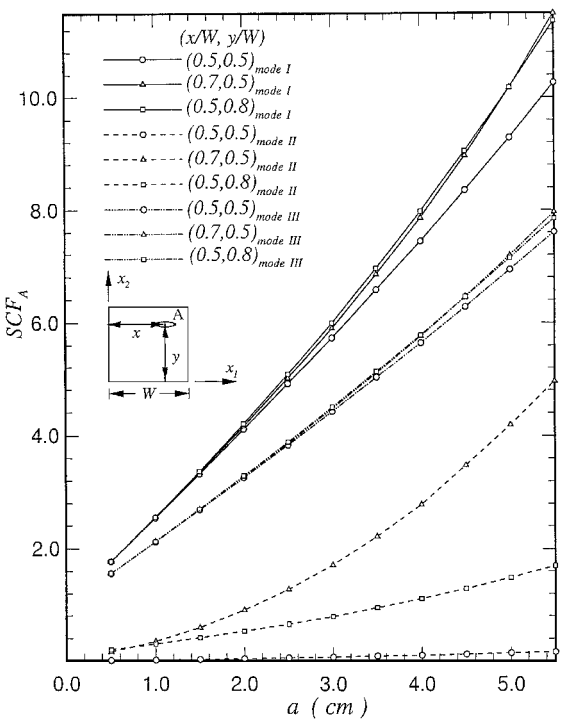

Fig. 4 Variation of SCF_A with respect to the hole size a and location $(x/W, y/W)$, where $\theta = 0$ and $b = 0.9$ cm.

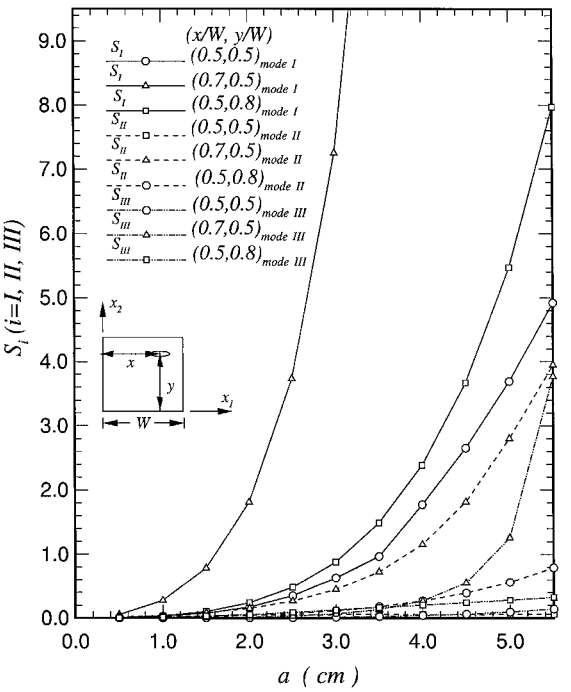

Fig. 6 Variation of the strain functions S_i (i = I, II, III) with respect to the hole size a and location $(x/W, y/W)$, where θ = 0 and $b = 0.9$ cm.

0.1 Pa when we calculate SCF_A of hole problems under mode II loading. For all of the other cases, the uniform loading σ_0 is kept to 1 Pa.

Variation with Respect to the Hole/Crack Orientation

Figures 7 and 8 show the variation of SCF_A, K_i, and S_i with respect to hole/crack orientation. The location of the hole/crack is fixed at $(x/W, y/W) = (0.5, 0.5)$, whereas the size is $a = 3$ cm, $b = 0.9$ cm for holes and $a = 3$ cm for cracks. As far as the sensitivity is concerned, the results of Figs. 7 and 8 show that there is no distinct difference between SCF_A/K_i and S_i. If we look at the promising candidate S_i from Fig. 8, we see that the most sensitive loading mode is no longer mode I considering the change of minor axis b. Moreover, S_i is very insensitive to the orientation under mode II loading. For example, S_i is about 0.2 when $\theta = 30$ and 80 deg and S_i is about 0.3 when $\theta = 60$ deg. It is difficult to identify θ when the variation of S_i is so small for the range $\theta = 30$–80 deg under mode II loading. However, if we change the loading to mode I, the orientation can be easily identified. Therefore, during the identification, the successive change of the loading mode is necessary for the advancement of the hole/crack search. This is also the key concept for the next section.

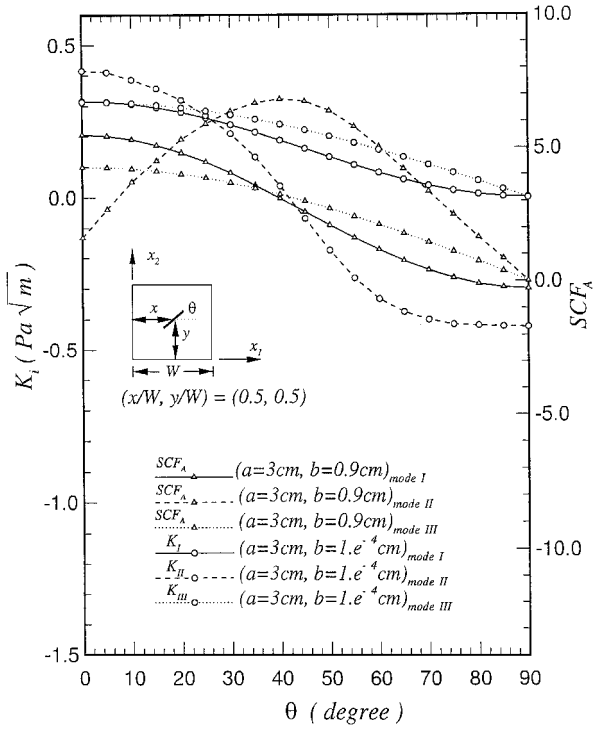

Fig. 7 Variation of SCF_A/K_i with respect to the hole/crack orientation θ.

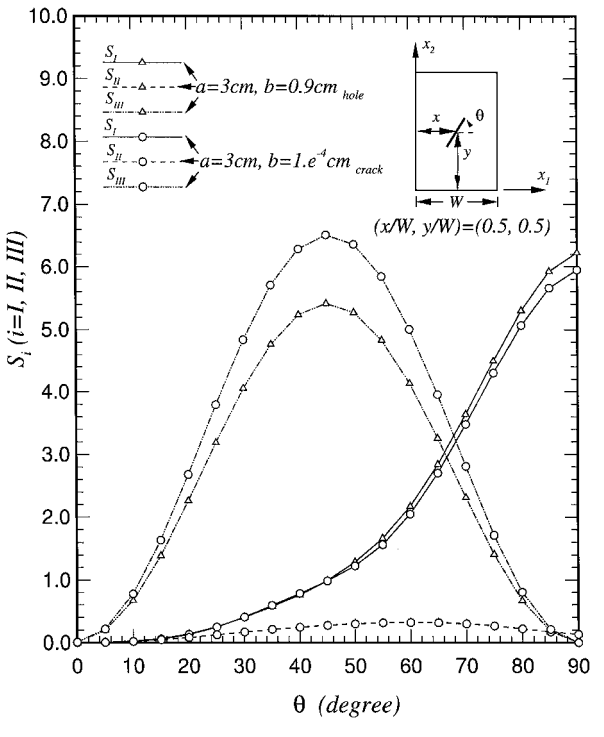

Fig. 8 Variation of the strain functions S_i (i = I, II, III) with respect to the hole/crack orientation θ.

III. Multistep Nonlinear Optimization

For the identification problems, the internal hole/crack boundary is unknown. A set of experimental measured strains is available on the remote boundary. If we restrict the identified hole to be elliptical and the identified crack to be straight, the identification problem becomes the determination of the hole/crack size (a^*, b^*), its orientation θ^*, and its centered position (x^*, y^*) based on the measured boundary strains ε^*_{ij}. To proceed with this kind of inverse problem, the technique of nonlinear optimization[22] will be applied. The public domain program COPES/ADS[35] is chosen to implement the optimization procedure, and the combination of methods used in this paper are the method of feasible direction plus polynomial interpolation.

From the discussion of Sec. II, we see that the insensitivity of the static strains to the hole/crack geometry and location may be overcome by the introduction of multiple loading modes. In other words, when the hole/crack cannot be identified by the static strains of a certain loading condition, we may switch the loading condition to another loading mode and improve the search for the hole/crack geometry and location. Repeat this process until the convergence criterion is satisfied. In practical situation, the pure mode loading condition may be induced by the embedded actuators, and the static strains may be measured by the embedded sensors. Based on this idea the repeated use of the different pure loading modes may not be too complicated to be achieved in real situations. With this concept, a multistep nonlinear optimization is designed as follows.

Minimize:

$$F_M = \sum_{k=1}^{L} \sum_{ij} \left(\frac{\varepsilon_{ij}}{\varepsilon^*_{ij}} - 1 \right)^2_k \tag{7}$$

for mode M (=I, II, III, or mixed) subject to

$$g_{ij} = \sum_{k=1}^{L} \left(\frac{\varepsilon_{ij}}{\varepsilon^*_{ij}} - 1 \right)^2_k - e < 0$$

where $ij = 11$, 12, and 22 for mode I and II; $ij = 13$ and 23 for mode III; and $ij = 11$, 12, 22, 13, and 23 for the mixed mode. Here

$$a_l < a < a_u, \qquad b_l < b < b_u, \qquad \theta_l < \theta < \theta_u$$

$$x_l < x < x_u, \qquad y_l < y < y_u$$

$$\max(a \cos|\theta|, b \sin|\theta|) - \min(x, W - x) < 0$$

$$\max(a \sin|\theta|, b \cos|\theta|) - \min(y, H - y) < 0 \tag{8}$$

If $F_M < F_0$, the convergence criterion is satisfied, and the program will be stopped. Otherwise, change mode M, decrease error tolerance e, and repeat the optimization stated in Eqs. (7) and (8) until the final result satisfies the convergence criterion or the maximum iteration number is exceeded. Refer to Fig. 9 for the flow chart of the multistep nonlinear optimization process.

In Eqs. (7) and (8), L is the number of sensors; a_l, b_l, θ_l, x_l, and y_l, and a_u, b_u, θ_u, x_u, and y_u are, respectively, the lower and upper bounds of design variables a, b, θ, x, and y. Because the crack is treated to be a special case of the elliptical holes with the minor axis b approaching zero, the lower bounds a_l and b_l are chosen to be a very small value 10^{-6} to include the conditions of cracks. The upper bounds of a and b are chosen to be reasonable and not too large, $a_u = b_u = W/4$. Additionally, to prevent a multivalue representation,

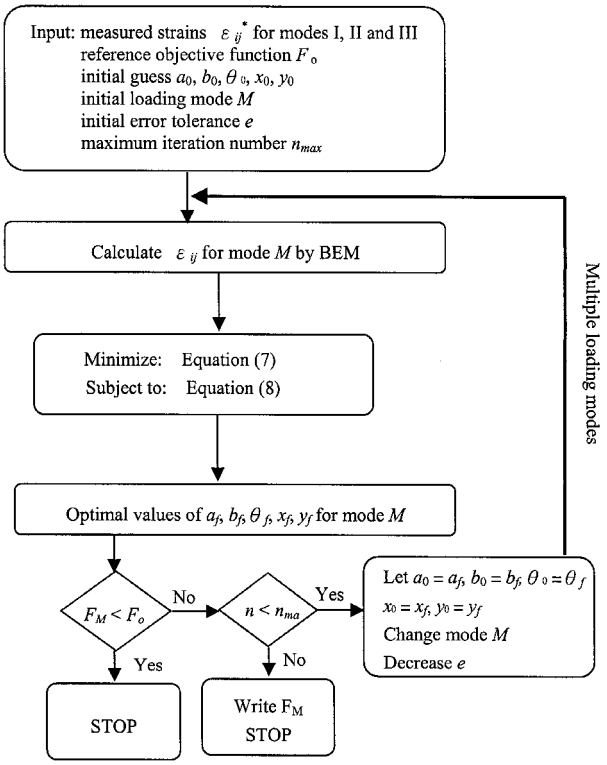

Fig. 9 Flowchart of nonlinear optimization with multiple loading modes.

the range of hole/crack orientation is set to $-\pi/2 < \theta < \pi/2$, that is, $\theta_l = -\pi/2$, $\theta_u = \pi/2$. If the sensors locate a distance d from the side of plate, the lower and upper bounds of hole/crack center location x, y are defined as $x_l = y_l = d$ and $x_u = W - d$, $y_u = H - d$. Sometimes a meaningless design may take place even if the design variables satisfy the bound conditions. For example, the hole or crack will locate outside the plate if $(x, y) = (0.1W, 0.1H)$ and $a = 0.2W$. The last two equations of Eq. (8) are added to enforce the hole/crack inside the plate. Except for the given constraints, the difference between the calculated strains and the measured strains cannot be too large. However, if each strain component of each sensor is set to be a constraint, there would be too many constraints, and the search for optimal value will be difficult to implement. Thus, to accomplish the nonlinear optimization efficiently, we only set the error sum (not individual error) of each strain component to be a constraint, which is shown in the first equation of Eq. (8). In case pure mode loadings are not easily induced in real situations, one may consider the general mixed mode loading conditions. In this case, all of the strain components are considered in our formulation.

A flow chart for the multistep nonlinear optimization process is shown in Fig. 9. At the beginning of iteration procedure, the measured strains ε_{ij}^* of each sensor for three pure loading modes should be input. In addition to these data, the other data necessary for the implementation of the optimal computer program are the reference objective function value F_0, the initial guess a_0, b_0, θ_0, x_0, and y_0, the initial loading mode M, the initial error tolerance e, and the maximum iteration number $n_{\max}$. During the iteration procedure, we need the values of the strains ε_{ij} corresponding to the assumed hole/crack geometry (a, b, θ, x, y) subjected to the pure loading mode M. In the following examples, these values are calculated by using the special boundary element introduced in Sec. II.

Just as the decision diamond block of Fig. 9 shows, if the optimal value of the objective function F_M is less than the critical value F_0 set by the users, the convergence criterion is satisfied, and the program will be stopped. A smaller value of F_0 makes the final identified result close to the target value, and consequently the time and iterations spent in the inverse calculation increase. The proper value of F_0 can make the result satisfactory and efficient. In the following examples, we choose $F_0 = 0.01$. The initial guess of a_0, b_0, θ_0, x_0, and y_0, and the initial loading mode M can then be given arbitrarily. The initial value of error tolerance e is usually chosen to be a relatively large value, for example, $e = 0.1$, to accelerate the optimization. When we finish one optimization procedure for a certain loading mode, we may decrease the tolerance e and change to the other loading mode. This process is repeated until the convergence criterion $F_M < F_0$ is satisfied and the hole/crack is identified, or the maximum iteration number is exceeded and the program is terminated. Note that no specific rules are set for the change of the loading mode and the decrease of the tolerance. They can be set arbitrarily just as the examples shown in Table 1.

Table 1 Effect of initial guess on the hole identification

Case	$2a/W$	$2b/W$	θ	x/W	y/W
1[a]					
Target value	0.1600	0.0600	0.785	0.4000	0.6000
Initial guess	0.1000	0.1500	0.349	0.6000	0.2000
Identified result	0.1352	0.0620	0.783	0.3980	0.5948
Error, %	15.5	3.26	0.31	0.49	0.86
2[b]					
Target value	0.1600	0.0600	0.785	0.4000	0.6000
Initial guess	0.0600	0.1200	1.047	0.6300	0.4200
Identified result	0.1494	0.0763	0.7786	0.3879	0.5866
Error, %	6.60	27.2	0.87	3.04	2.24
3[c]					
Target value	0.1600	0.0600	0.785	0.4000	0.6000
Initial guess	0.0800	0.0300	0.262	0.3000	0.2000
Identified result	0.1497	0.0619	0.7475	0.4142	0.6534
Error, %	6.44	3.15	4.83	3.56	8.89

[a]Sequence of loading mode I → II → III → I → II, reduction of error tolerances 1 → 0.5 → 0.1 → 0.05 → 0.01, objective function 1.705e−3, and 364 iterations.
[b]Sequence of loading mode I → III → II → I → II, reduction of error tolerances $10^{-3} \to 10^{-4} \to 10^{-5} \to 10^{-6} \to 10^{-7}$, objective function 8.021e−3 and 276 iterations.
[c]Sequence of loading mode II → III → I → III → II → I → III → II → III → I, reduction of error tolerances 1 → 0.5 → 0.1 → 0.05 → 0.01 → 0.005 → 0.001 → 0.0005 → 0.0001 → 0.00005, objective function 7.832e−3, and 571 iterations.

Example 1: Hole Identification

To show the effect of multiple loading modes, a hole identification example has been done by using only one loading mode or multiple loading modes. The geometry and sensor location of the plate is shown in Fig. 1. The material of the plate is chosen to be orthotropic with the properties as given in Sec. II. The strains measured on the eight sensor locations subjected to three different loading modes are provided by numerical simulation and are shown in Table 2. To avoid double usage of the computational model in both forward and inverse problems, the measured data are generated by commercial finite element code IDEAS with eight-node two-dimensional element meshed by 1764 elements and 4860 nodes. Before running our identification program, the following initial values are given: $F_0 = 0.01$, $a_0 = 0.129$ cm, $b_0 = 0.09$ cm, $\theta_0 = 0.262$, $x_0 = 2.4$ cm, $y_0 = 0.6$ cm, $M = I$, $e = 0.1$, and $n_{\max} = 1500$. From Table 3 we see that if we use mode I only, the convergence criterion $F_M < F_0$ will not be satisfied even when we reduce the tolerance e to 1.e−6 and the iteration number is equal to 1500. On the other hand, by reducing the tolerance e successively for different loading modes, the convergence criterion is easily satisfied, and the final identified result is close to the target within 10% error.

Note that the errors of the identified result are defined as $|(s - s^*)/s^*| \times 100\%$ for $s = a, b, \theta, x$, or y, if s^* is not zero. The symbol with superscript $*$ denotes the target value. If s^* is equal to zero such as the horizontal orientation whose $\theta^* = 0$, the definition will be modified as $|(\theta - \theta^*)/\pi| \times 100\%$.

Example 2: Crack Identification

Because of the localized characteristics of cracks, only the size of the crack was identified through the use of the stress intensity factor subjected to only one loading mode.[23] In this example, we try to use the hole identification program to identify a crack to see whether our program has the ability to identify a hole with zero minor axis. Figure 10 shows the identified results by using only one loading mode (mode I), two loading modes (modes II + III), and three loading modes (modes I + II + III). The results clearly show

Table 2 Strains measured on the eight sensor locations subjected to three loading modes[a]

	Tensile mode I			Shearing mode II			Tearing mode III	
Sensor	ε^*_{11} ($\times 10^{-5}$)	ε^*_{12} ($\times 10^{-4}$)	ε^*_{22} ($\times 10^{-4}$)	ε^*_{11} ($\times 10^{-4}$)	ε^*_{12} ($\times 10^{-4}$)	ε^*_{22} ($\times 10^{-3}$)	ε^*_{13} ($\times 10^{-5}$)	ε^*_{23} ($\times 10^{-4}$)
1	0.6344	−0.2783	0.3493	−0.8464	−0.2297	0.3105	−0.0095	0.5226
2	−0.2353	−0.2031	0.3811	0.1659	−0.4525	0.1966	0.0108	0.5281
3	−0.9779	−0.1756	0.5056	0.6531	−0.7211	0.1433	0.0083	0.5193
4	−0.1200	−0.2529	0.4567	0.5064	0.0210	0.0401	−0.0571	0.5154
5	0.6631	−0.2778	0.3170	0.5709	0.1531	0.0469	−0.0211	0.5210
6	−0.1876	−0.1965	0.3616	0.3137	0.0327	−0.0258	0.0146	0.5232
7	−0.6884	−0.1951	0.5011	0.1077	0.3006	−0.1062	0.0056	0.5182
8	0.1171	−0.2571	0.4373	−0.5567	0.3735	0.0314	−0.0009	0.5167

[a]Hole geometry and location are $2a/W = 0.114$, $2b/W = 0.02$, $\theta = 0.698$, $x/W = 0.467$, and $y/W = 0.533$.

Table 3 Effect of multiple loading modes on the hole identification

Loading mode	Mode	Tolerance	Iteration	$2a/W$	$2b/W$	θ	x/W	y/W	Objective function
1									
Initial guess				0.0860	0.0600	0.262	0.8000	0.2000	
Identified result	I	1e−6	1500	0.0618	0.0281	0.661	0.4785	0.5865	5.72e−2
Target value				0.1140	0.0200	0.698	0.4667	0.5333	
Error, %				45.8	40.5	5.30	2.53	9.98	
Multiple									
Initial guess				0.1000	0.0640	0.2618	0.3000	0.7000	
Identified result	II	1e−1	75	0.2348	0.2229	0.2772	0.6619	0.7565	48.1
	I	5e−2	36	0.0200	0.0258	0.7023	0.4670	0.5404	8.414e−2
	III	1e−2	25	0.0337	0.0475	0.9690	0.4555	0.5249	1.117
	I	5e−3	62	0.1251	0.0208	0.7175	0.4595	0.5011	4.935e−3
Target value				0.1140	0.0200	0.698	0.4667	0.5333	
Error, %				9.77	3.96	2.77	1.55	6.05	

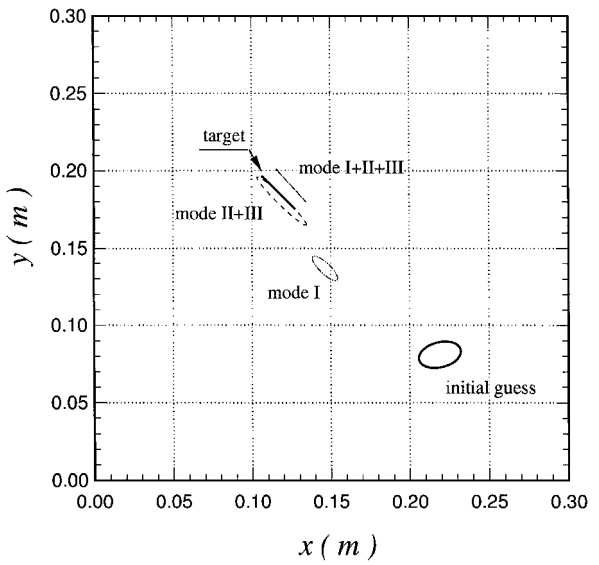

Fig. 10 Effect of multiple loading modes on the crack identification.

that by using mode I only, the identified result is far away from the target and is still a hole. By using modes II + III, the identified result is just beside the target and is near a narrow ellipse. By using modes I + II + III, the profile of a crack is distinctly identified, and the location is near to the target.

IV. Hole/Crack Identification

The feasibility of combining the concept of multiple loading modes with the technique of nonlinear optimization for hole/crack identification has been shown in the preceding section. In this section, we prove numerically that our program is stable with respect to the following factors: initial guess of the design variables, initial loading mode, and initial error tolerance. We also show that our program is general enough to cover the following cases: any kind of homogeneous linear elastic materials (such as isotropic, orthotropic, anisotropic, piezoelectric materials, etc.), and any kind of hole profiles (such as ellipse, crack, polygon, nonhole, i.e., perfect plate, etc.). The other influential factors that are important for future applications and that will also be discussed are the number of design variables, the tolerance of measured strains, the spacing of sensors, the arrangement of sensors, and the mixed mode loading condition, etc.

Stability

To show the stability of our method through theoretical derivation is difficult because of the intractability of explicit presentation for the inverse problem. However, it is important for an inverse problem to have a stable result not affected by the initial guesses. To prove this numerically, many different examples have been tested.[36] The results presented by Liang showed that the identification is always stable and accurate no matter what initial guess of the design variables, initial loading mode, and initial error tolerance are provided. Moreover, the sequence of the loading mode and its corresponding error tolerance can also be provided arbitrarily. Unlike the accuracy, the efficiency is usually dependent on the initial guess, starting loading mode, and the sequence of the loading modes. However, from the numerical data, it is difficult to find a rule for the acceleration of the searching speed. To save space here, only three examples are collected in Table 1 to show the stability of our method. For a clear picture of its progress and success, the associated graphic representation of the iteration procedure is shown in Fig. 11 for case 3 of Table 1.

Generality

Structural Materials

During the optimization process, the strain values corresponding to the assumed hole/crack geometry and location are calculated by using the special boundary element introduced in Sec. II. Hence, the inclusion of the other kinds of materials in the present program depends on the extension of the boundary element method. Because the fundamental solution used in this element is derived based on Stroh's formalism[30] (see also Ref. 31) for anisotropic elasticity, it may be applied to any kinds of anisotropic materials including isotropic and orthotropic materials. However, note that isotropic materials belong to the category of degenerate materials whose material eigenvalues

Table 4 Hole identification of various structural materials

Case	$2a/W$	$2b/W$	θ	x/W	y/W
Isotropic					
Initial guess	0.1420	0.0260	1.134	0.3700	0.6300
Identified result[a]	0.1234	0.0962	0.001	0.5391	0.4909
Target value	0.1220	0.0960	0.000	0.5400	0.4900
Error, %	1.11	0.22	0.04	0.16	0.17
Anisotropic					
Initial guess	0.0440	0.0260	0.2620	0.3000	0.8000
Identified result[b]	0.1246	0.0782	0.7834	0.6282	0.4350
Target value	0.1260	0.0820	0.7854	0.6200	0.4300
Error, %	1.14	4.65	0.26	1.33	1.15
Piezoelectric					
Initial guess	0.1240	0.0667	0.5236	0.6300	0.3400
Identified result[c]	0.0904	0.0395	1.0769	0.4286	0.5812
Target value	0.0820	0.0460	1.0472	0.4500	0.6000
Error, %	10.2	14.1	2.84	4.75	3.13

[a]Objective function $8.602e{-}3$.
[b]Objective function $2.920e{-}3$.
[c]Objective function $2.336e{-}3$.

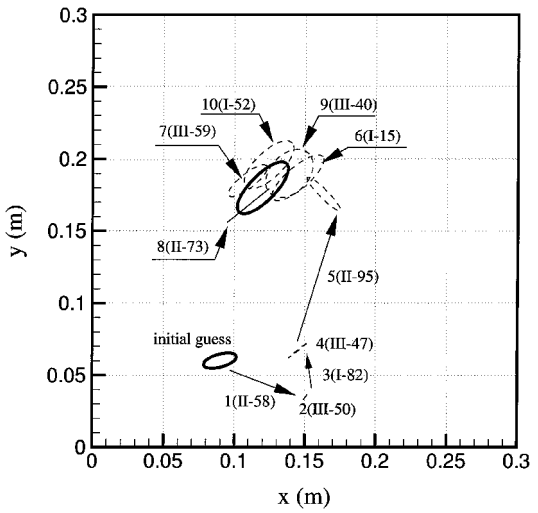

N(M-n) : the Nth step with loading mode M and n iterations.

Fig. 11 Iteration procedure for the hole identification.

are repeated.[31,37] When applying our program to this kind of materials, small perturbation of the material constants should be introduced.[21] For piezoelectric materials, the related boundary element has been developed in our previous study.[25] Because the case using the orthotropic materials has been executed successfully and presented in Tables 1 and 3, Table 4 shows the other three cases using the materials given in Sec. II. The identified results of the isotropic and anisotropic materials are within 5% error of the target value. For piezoelectric materials, the maximum error is 14.1%, which is acceptable.

Hole Profiles

It is not unusual to find a nonelliptical hole in structural materials. If the exact profile of a hole is not the main concern for the usual investigation, we may try to use the elliptical hole to match any unknown holes. Figure 12 shows the identified result for a triangular hole, which is acceptable from the practical point of view. Note that in our program, the measured strains are simulated by the boundary element for polygonal holes.[28]

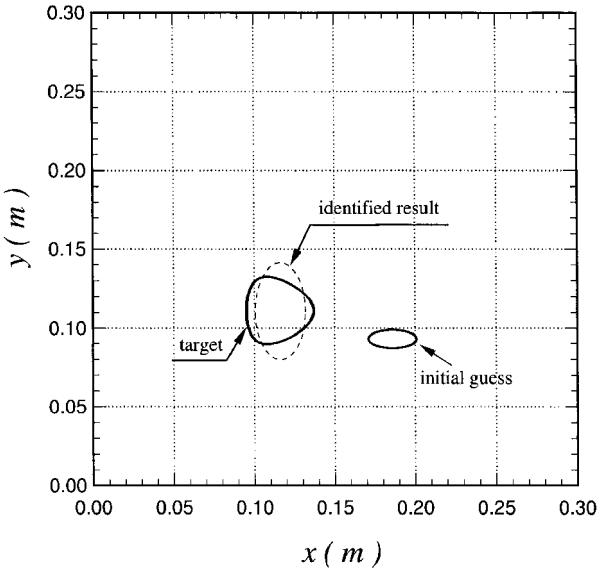

Fig. 12 Triangular hole identification.

Besides nonelliptical holes, it is also interesting to test our program on a perfect plate, that is, a plate without holes. In actual implementation, we found that our identified results reach the minimum values of the hole size a and b, whereas for the location (x, y) and orientation θ, unstable values are obtained. This is reasonable because our measured strains are provided for the case that no holes exist in the plate.

Influential Factors

Number of Design Variables

As shown in Example 2 of Sec. III, the crack may be identified as a narrow elliptical hole when the design variables include the minor axis b of the ellipse. This approach is reasonable if the profiles of the defects of the structural materials are unknown in advance. However, if the purpose of the identification is restricted to crack identification, we may reduce the number of design variables by one. That is, only a, θ, x, and y are used as the design variables. This will speed the optimization and increase the accuracy. To save space, the results are not shown here. One may refer to Liang[36] for the detailed presentation.

Tolerance of Measured Strains

In real applications, it is unavoidable to have some errors for the measured strains. To make the data more like real measurement data, some of the measured strains in Table 2 are randomly selected to have 5, 10, 15, and 20% measured errors. When these values are input into our program, the identified results are obtained and shown in Fig. 13. The mean square error (MSE) shown in the upper-right-hand portion of Fig. 13 is defined as

$$\mathrm{MSE} = \sqrt{\frac{1}{5}\left[\left(\frac{a}{a^*}-1\right)^2+\left(\frac{b}{b^*}-1\right)^2+\left(\frac{\theta}{\theta^*}-1\right)^2+\left(\frac{x}{x^*}-1\right)^2+\left(\frac{y}{y^*}-1\right)^2\right]}\times 100\% \tag{9}$$

Combined with several other results shown by Liang,[36] we see that, when the measured errors increase, the errors of the identified results increase but not necessarily in a linear proportional relation, which is expected and reasonable.

Spacing of Sensors

Table 5 shows the effect of sensor spacing on the hole identification. To know its influence on the efficiency and accuracy, two holes with different sizes are considered. One is 10 times larger than the other for both major and minor axes. The location and orientation are the same for these two holes. In both cases, four different

Table 5 Effect of sensor spacing on the hole identification

Number of sensors	$\Delta l/W$	Result	$2a/W$	$2b/W$	θ	x/W	y/W	CPU time, s
			Large hole					
		Target value	0.4400	0.2200	1.047	0.4000	0.6000	
16	0.200	Identified result	0.4490	0.2188	1.042	0.3944	0.5914	1620.0
		Error, %	2.05	0.57	0.52	1.41	1.44	
12	0.267	Identified result	0.4226	0.2266	1.048	0.4211	0.6353	1306.2
		Error, %	3.96	3.01	0.06	5.28	5.89	
8	0.400	Identified result	0.4412	0.2307	1.021	0.3921	0.5787	910.1
		Error, %	0.26	4.86	2.51	1.97	3.55	
4	0.800	Identified result	0.4446	0.2172	1.039	0.3942	0.5878	873.6
		Error, %	1.05	1.27	0.82	1.46	2.04	
			Small hole					
		Target value	0.0440	0.0220	1.047	0.4000	0.6000	
16	0.200	Identified result	0.0441	0.0214	1.062	0.4180	0.5746	6865.2
		Error, %	0.26	2.68	1.43	4.50	4.23	
12	0.267	Identified result	0.0401	0.0206	1.048	0.4003	0.6147	5443.2
		Error, %	8.86	6.44	0.10	0.08	2.45	
8	0.400	Identified result	0.0426	0.0214	1.043	0.3991	0.5718	2960.5
		Error, %	3.14	2.73	0.42	0.23	4.70	
4	0.800	Identified result	0.0477	0.0258	1.046	0.3947	0.6244	2265.5
		Error, %	8.42	17.1	0.08	1.32	4.06	

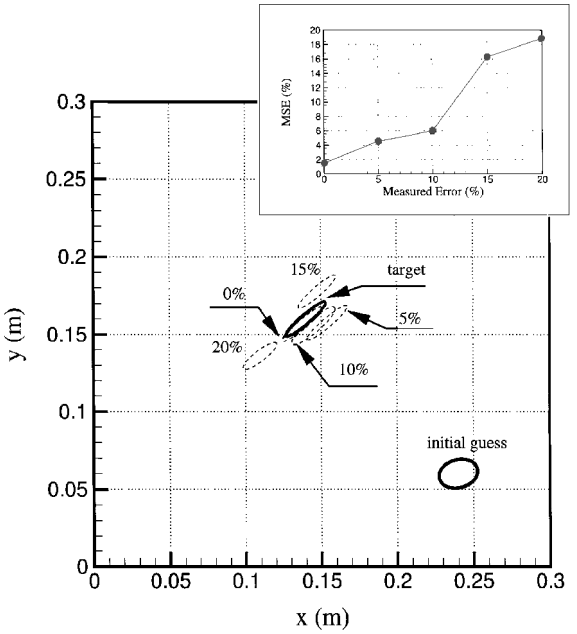

Fig. 13 Hole identification with measured error.

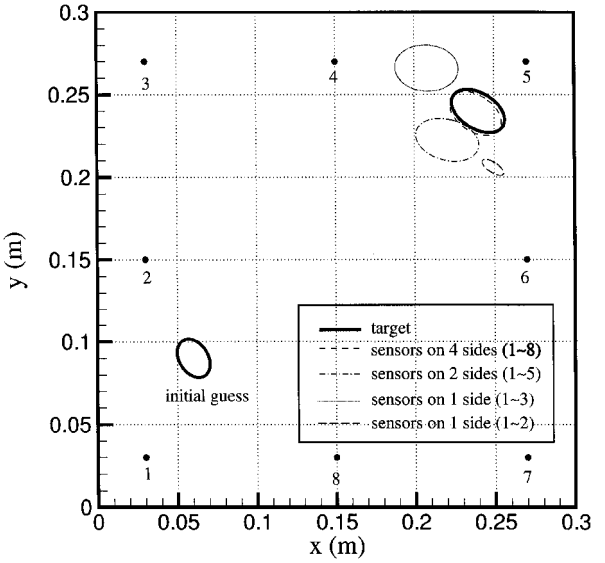

Fig. 14 Hole identification with different sensor arrangements.

sensor spacings are arranged. Their corresponding sensor numbers are 4, 8, 12, and 16. The results show that the larger hole is easier to be identified (less CPU time), which is expected. As regards to the sensor spacing, it seems that fewer sensors (or wide spacing) may reduce the searching time. However, the error of the minor axis b by using only four sensors for the smaller hole reaches 17.1%, which is too high compared with the other sensor spacing arrangements. Note that all of the data presented in Table 5 satisfy the convergence criterion set in Fig. 9. The reason why the error is still high may be due to the fewer constraints for the fewer sensors. That is, even though the result is not accurate enough, the constraints at the fewer selected sensors have been satisfied.

We see that the CPU time for eight sensors is just a little longer than that for four sensors. This may be explained by the increase of the iteration number for fewer sensors, although their corresponding searching time for each iteration may decrease. When considerating both the efficiency and accuracy, the optimal sensor spacing ($\Delta l/W$) is recommended to be 0.4, which corresponds to eight sensors for the present cases.

Arrangement of Sensors

All of the examples considered use measurements surrounding the hole/crack. It is interesting to see what the results would be if measurements could be taken on only one or two sides of the specimen. Figure 14 shows that although the results identified by using sensors located on only one or two sides of the specimen are not as good as the results identified by using sensors around the perimeter, they are still in the neighborhood of the target. In terms of the MSE defined in Eq. (9), the errors are 2.1% for four sides with eight sensors, 14.9% for two sides with five sensors, 25.3% for one side with three sensors, and 41.9% for one side with only two sensors. If we raise the convergence criterion by decreasing the critical value of F_0, the results for fewer sensors may be improved. For example, MSE = 3% for five sensors with $F_0 = 0.001$, MSE = 14.6% for three sensors with $F_0 = 0.0001$, and MSE = 24.9% for two sensors with $F_0 = 0.00001$ (the results shown in Fig. 14 are identified by setting $F_0 = 0.01$). However, the searching time and iteration numbers in the inverse calculation will also increase. Hence, it is still suggested that the sensors be located around the perimeter unless there is difficulty in real applications. In that case, the convergence criterion should be raised.

Mixed-Mode Loading Conditions

The preceding examples are executed by the standard pure loading modes such as tensile, shearing, and tearing modes. In practice, mixed mode loading conditions may occur. To test the applicability of the mixed mode loading conditions, three independent vectors are

Table 6 Hole identification with arbitrary mixed-mode loadings

Mode	Iteration	$2a/W$	$2b/W$	θ	x/W	y/W	Objective function
			Initial guess				
		0.0600	0.0480	0.2618	0.8000	0.2400	
			Identified result				
C	34	0.0200	0.0764	1.3067	0.4998	0.5844	$6.085e{+}0$
B	169	0.1205	0.1041	1.2553	0.4623	0.5429	$2.355e{-}1$
A	160	0.1383	0.1141	1.2790	0.4693	0.5348	$2.609e{-}1$
B	36	0.1352	0.1103	1.2814	0.4644	0.5326	$1.517e{-}1$
C	57	0.1265	0.1081	1.3006	0.4666	0.5394	$9.358e{-}3$
			Target value				
		0.1240	0.1120	1.3090	0.4700	0.5400	
			Error, %				
		2.03	3.52	0.64	0.72	0.10	

arbitrarily selected to make mixed loading modes A, B, and C. The forces are applied on the upper and lower edges of the rectangular plate and are uniformly distributed along the edge with nonzero traction values as $\{\sigma_{12}\ \sigma_{22}\ \sigma_{23}\}_A = \{0.93\ 0.30\ 0.21\}\sigma_0$, $\{\sigma_{12}\ \sigma_{22}\ \sigma_{23}\}_B = \{0.42\ 0.83\ 0.38\}\sigma_0$, and $\{\sigma_{12}\ \sigma_{22}\ \sigma_{23}\}_C = \{0.40\ 0.23\ 0.89\}\sigma_0$. From the results of Table 6, we can conclude that it is not necessary to have standard pure loading modes to identify a hole or crack. The identification result may be precise as long as the mixed loading modes are independent of each other. The accurate result of this example completes the concept of multiple loading modes because the loading modes are not restricted to pure loading modes.

V. Conclusions

The feasibility of identifying a hole/crack by using only the data from static deformation is confirmed. The data chosen from the static deformation are the most convenient and easily obtainable data, static strains on the remote boundary. The breakthrough that leads us to identify a hole/crack is the introduction of the concept of multiple loading modes. When this concept is combined, a multistep nonlinear optimization process is designed. Through this process the optimal result of each step can be used as an initial guess of the next step under a different loading mode, until the final result satisfies our convergence criterion. Thus, not only the hole/crack size but also the location and orientation can be identified.

From the numerical examples shown, we see that our method for hole/crack identification is stable and accurate for the model problem considered, which shows that the method has promise for more complex problems. Moreover, our program is general enough to cover any kind of homogeneous linear anisotropic elastic material including piezoelectric materials. If the exact profile of the hole is not the main concern for the usual investigation, any nonelliptical hole can also be matched approximately by using an elliptical hole. If the investigation is restricted to crack identification, fewer designed variables can be used to speed the optimization. As expected, the measurement error of static strains will influence the identified results proportionally. As to the spacing of sensors, according to our numerical data we recommend the ratio of spacing to the plate width be 0.4. Moreover, the sensors could be put on only one, two, or three sides of the specimen. If the pure loading mode is not easily actuated, any kind of independent mixed loading modes can be used. After the hole/crack is identified, the stress concentration factor for holes or the stress intensity factors for cracks can easily be obtained from the boundary data using our recently derived formula.[28] Although there are many advantages, the total CPU time is still too long to be applied to online identification. To achieve this goal, we will apply this concept to artificial neural networks in our future work.

Acknowledgments

The authors would like to thank the National Science Council for support through Grants NSC 85-2212-E006-059 and NSC 87-2212-E-006-090.

References

[1]Bray, D. E., and Stanley, R. K., *Nondestructive Evaluation—A Tool in Design, Manufacturing and Service*, McGraw–Hill, New York, 1993, pp. 45–552.

[2]Qian, G. L., Gu, S. N., and Jiang, J. S., "The Dynamic Behavior and Crack Detection of a Beam with a Crack," *Journal of Sound and Vibration*, Vol. 138, No. 2, 1990, pp. 233–243.

[3]Rizos, P. F., Aspragathos, N., and Dimarogonas, A. D., "Identification of Crack Location and Magnitude in a Cantilever Beam from the Vibration Modes," *Journal of Sound and Vibration*, Vol. 138, No. 3, 1990, pp. 381–388.

[4]Ricles, J. M., and Kosmatka, J. B., "Damage Detection in Elastic Structures Using Vibratory Residual Forces and Weighted Sensitivity," *AIAA Journal*, Vol. 30, No. 9, 1992, pp. 2310–2316.

[5]Ratan, S., Baruh, H., and Rodriguez, J., "On-Line Identification and Location of Rotor Cracks," *Journal of Sound and Vibration*, Vol. 194, No. 1, 1996, pp. 67–82.

[6]Shen, M. H. H., and Taylor, J. E., "An Identification Problem for Vibrating Cracked Beams," *Journal of Sound and Vibration*, Vol. 150, No. 3, 1991, pp. 457–484.

[7]Sato, H., "Free Vibration of Beams with Abrupt Changes of Cross-Section," *Journal of Sound and Vibration*, Vol. 89, No. 1, 1993, pp. 59–64.

[8]Banks, H. T., and Inman, D. J., "On Damping Mechanisms in Beams," *Journal of Applied Mechanics*, Vol. 58, No. 3, 1991, pp. 716–723.

[9]Banks, H. T., Inman, D. J., Leo, D. J., and Wang Y., "An Experimentally Validated Damage Detection Theory in Smart Structures," *Journal of Sound and Vibration*, Vol. 191, No. 5, 1996, pp. 859–880.

[10]Chen, D. H., and Nisitani, H., "Detection of a Crack by Body Force Method," *Engineering Fracture Mechanics*, Vol. 45, No. 5, 1993, pp. 671–685.

[11]Hsieh, S. C., and Mura, T., "Nondestructive Cavity Identification in Structures," *International Journal of Solids and Structures*, Vol. 30, No. 12, 1993, pp. 1579–1587.

[12]Atkinson, C., and Aparicio, N. D., "An Inverse Problem Method for Crack Detection in Elastic Materials Under Anti-Plane Strain," *Proceedings of the Royal Society of London, Series A: Mathematical and Physical Sciences*, Vol. 445, No. 1925, 1994, pp. 637–652.

[13]Liu, P. L., "Parametric Identification of Plane Frames Using Static Strains," *Proceedings of the Royal Society of London, Series A: Mathematical and Physical Sciences*, Vol. 452, No. 1944, 1996, pp. 29–45.

[14]Liu, P. L., and Lin, H. T., "Direct Identification of Non-Uniform Beams Using Static Strains," *International Journal of Solids and Structures*, Vol. 33, No. 19, 1996, pp. 2775–2787.

[15]Sanayei, M., and Onipede, O., "Damage Assessment of Structures Using Static Test Data," *AIAA Journal*, Vol. 29, No. 7, 1991, pp. 1174–1179.

[16]Kubo, S., Ohji, K., Nakatsuka, K., and Fujito, H., "An Application of Optimization Techniques to Measurement of Two- and Three-Dimensional Cracks by the Electric Potential CT Method," *Inverse Problems in Engineering: Theory and Practice*, American Society of Mechanical Engineers, Fairfield, NJ, 1993, pp. 163–169.

[17]Bryan, K., and Vogelius M., "A Computational Algorithm to Determine Crack Locations from Electrostatic Boundary Measurements. The Case of Multiple Cracks," *International Journal of Engineering Science*, Vol. 32, No. 4, 1994, pp. 579–603.

[18]Brebbia, C. A., Telles, J. C. F., and Wrobel, L. C., *Boundary Element Techniques—Theory and Applications in Engineering*, Springer-Verlag, New York, 1984, pp. 177–236.

[19]Nishimura, N., and Kobayashi, "A Boundary Integral Equation Method for an Inverse Problem Related to Crack Detection," *International Journal for Numerical Methods in Engineering*, Vol. 32, No. 5, 1991, pp. 1371–1387.

[20]Zeng, X., and Saigal, S., "An Inverse Formulation with Boundary Elements," *Journal of Applied Mechanics*, Vol. 59, No. 4, 1992, pp. 835–840.

[21]Hwu, C., and Yen, W. J., "Green's Functions of Two-Dimensional Anisotropic Plates Containing an Elliptic Hole," *International Journal of Solids and Structures*, Vol. 27, No. 13, 1991, pp. 1705–1719.

[22]Vanderplaats, G. N., *Numerical Optimization Techniques for Engineering Design: With Applications*, McGraw–Hill, New York, 1984.

[23]Liang, Y. C., and Hwu, C., "Analysis and Identification of Cracks in Piezoelectric Materials," *Proceedings of the Tenth International Conference on Composite Materials*, Woodhead Publishing, Ltd., Cambridge, England, U.K., 1995, pp. V315–V322.

[24]Hwu, C., and Liao, C. Y., "A Special Boundary Element for the Problems of Multi-Holes, Cracks and Inclusions," *Computers and Structures*, Vol. 51, No. 1, 1994, pp. 23–31.

[25]Liang, Y. C., and Hwu, C., "Electromechanical Analysis of Defects in Piezoelectric Materials," *Smart Materials and Structures*, Vol. 5, No. 2, 1996, pp. 314–320.

[26]Hwu, C., "Anisotropic Plates With Various Openings Under Uniform Loading or Pure Bending," *Journal of Applied Mechanics*, Vol. 57, No. 4, 1990, pp. 700–706.

[27] Hwu, C., "Polygonal Holes in Anisotropic Media," *International Journal of Solids and Structures*, Vol. 29, No. 19, 1992, pp. 2369–2384.

[28] Hwu, C., and Liang, Y. C., "Evaluation of Stress Concentration Factors and Stress Intensity Factors from Remote Boundary Data," *International Journal of Solids and Structures*, Vol. 37, No. 41, 2000, pp. 5957–5972.

[29] Hwu, C., "A Cubic Boundary Element for Two-Dimensional Composite Plates Containing Holes," *Twelfth International Conference on Composite Materials*, Woodhead Publishing, Ltd., Cambridge, England, U.K., 1999.

[30] Stroh, A. N., "Dislocations and Cracks in Anisotropic Elasticity," *Philosophical Magazine*, Vol. 7, No. 3, 1958, pp. 625–646.

[31] Ting, T. C. T., *Anisotropic Elasticity—Theory and Applications*, Oxford Science, Oxford, 1996, pp. 134–163.

[32] Hwu, C., "A New BEM for Two-Dimensional Anisotropic Elastic Solids Containing Multiple Holes, Cracks and Inclusions," *Discontinuous Materials and Structures*, edited by M. B. Bush, Advances in Boundary Element Series, WIT Press/Computational Mechanics, Southampton, England, U.K., 1999, Chap. 2.

[33] Broek, D., *Elementary Engineering Fracture Mechanics*, Noordhoff International, Leyden, The Netherlands, 1974, pp. 67–73.

[34] Timoshenko, S. P., and Goodier, J. N., *Theory of Elasticity*, McGraw–Hill, New York, 1970.

[35] Vanderplaats, G. N., "A Fortran Control Program for Engineering Synthesis (COPES) Using the Automated Design Synthesis (ADS) Optimization Program," Engineering Design Optimization, Santa Barbara, CA, 1985.

[36] Liang, Y. C., "Hole/Crack Identification in Two-Dimensional Composite Structures," Ph.D. Dissertation, Inst. of Aeronautics and Astronautics, National Cheng-Kung University, Tainan, Taiwan, ROC, 1999.

[37] Ting, T. C. T., and Hwu, C., "Sextic Formalism in Anisotropic Elasticity for Almost Non-Semisimple Matrix N," *International Journal of Solids and Structures*, Vol. 24, No. 1, 1988, pp. 65–76.

S. Saigal
Associate Editor